Scalar-pseudoscalar pair production at the Large Hadron Collider at NLO+NLL accuracy in QCD*

He-Yi Li(李和意)[1,2] Ren-You Zhang(张仁友)[1,2†] Yu Zhang(张宇)[3,4] Wen-Gan Ma(马文淦)[1,2]
Ming-Ming Long(龙明明)[1,2] Shu-Xiang Li(李书香)[1,2]

[1]State Key Laboratory of Particle Detection and Electronics, University of Science and Technology of China, Hefei 230026, China
[2]Department of Modern Physics, University of Science and Technology of China, Hefei 230026, China
[3]Institutes of Physical Science and Information Technology, Anhui University, Hefei 230601, China
[4]School of Physics and Materials Science, Anhui University, Hefei 230601, China

Abstract: We thoroughly investigate both transverse momentum and threshold resummation effects on scalar-pseudoscalar pair production via quark-antiquark annihilation at the 13 TeV Large Hadron Collider at QCD NLO+NLL accuracy. A factorization method is introduced to properly supplement the soft-gluon (threshold) resummation contribution from parton distribution functions to the resummed results obtained by the Collins-Soper-Sterman resummation approach. We find that the impact of the threshold-resummation improved PDFs is comparable to the resummation effect of the partonic matrix element and can even predominate in high invariant mass regions. Moreover, the loop-induced gluon-gluon fusion channel in the type-I two-Higgs-doublet model is considered in our calculations. The numerical results show that the electroweak production via quark-antiquark annihilation dominates over the gluon-initiated QCD production by 1 ~ 2 orders of magnitude.

Keywords: scalar-pseudoscalar pair production, two-Higgs-doublet model, resummation

DOI: 10.1088/1674-1137/ac23d2

I. INTRODUCTION

Primary tasks at the Large Hadron Collider (LHC) include the precision test of the standard model (SM) and the search for new physics beyond the SM (BSM). Since the discovery of the 125 GeV Higgs boson by both ATLAS and CMS collaborations at the LHC in 2012 [1, 2], the SM has become the most successful theory in describing the interactions of fundamental particles. However, the discovery of this SM-like Higgs boson is merely one step toward fully investigating the electroweak symmetry breaking (EWSB). As is well known, the theoretical predictions of the SM are not always compatible with experimental observations, such as the dark matter in the universe, the oscillation of neutrinos, the huge hierarchy between electroweak and Planck scales, and the fine-tuning problem of Higgs mass. These conceptional and experimental difficulties encountered by the SM imply the existence of new physics beyond the SM.

We may extend the SM by enlarging its gauge symmetry and/or introducing much more gauge multiplets to construct a new physics model. Among all the BSM theories, the two-Higgs-doublet model (2HDM) [3] is one of the simplest extensions of the SM. The Higgs sector responsible for the EWSB consists of two complex scalar isospin doublets, and the minimal supersymmetric standard model is a particular realization of the 2HDM. After EWSB, the three Goldstone modes $G^{\pm}$ and G^0 in the Higgs sector of the 2HDM are absorbed by the weak gauge bosons $W^{\pm}$ and Z^0, respectively, providing the longitudinal polarizations of $W^{\pm}$ and Z^0. The remaining five mass eigenstates of the Higgs sector are the so-called $\mathcal{CP}$-even Higgs bosons h^0 and H^0, $\mathcal{CP}$-odd Higgs boson A^0, and charged Higgs bosons $H^{\pm}$.

Clearly, any discovery of a BSM Higgs boson will be an evidence for the existence of a new Higgs sector. At the LHC, the neutral Higgs bosons of the 2HDM can be produced both singly and in identical or mixed pairs. The dominant mechanism for single production of neutral Higgs bosons is gluon-gluon fusion. Concerning scalar-pseudoscalar pairs, the electroweak production via quark-antiquark annihilation, $pp \to q\bar{q} \to Z^* \to H^0A^0/h^0A^0$, can dominate over the QCD production via gluon-gluon fusion [4, 5], even by orders of magnitude. Considerable efforts have been devoted to search for BSM neutral Higgs bosons. Particularly, the exotic decays of heavy scalar

Received 30 May 2021; Accepted 6 September 2021; Published online 13 October 2021

* Supported in part by the National Natural Science Foundation of China (11775211, 12061141005, 11805001, 11935001) and the CAS Center for Excellence in Particle Physics (CCEPP)

† E-mail: zhangry@ustc.edu.cn, corresponding author

(pseudoscalar), such as $H^0 \to A^0Z^0$ ($A^0 \to H^0Z^0$), have attracted attention at the LHC in recent years [6, 7]. The scalar-pseudoscalar pair production is dominated by the Drell-Yan channel; it is an ideal process to investigate the Higgs gauge coupling $g_{H^0A^0Z^0}/g_{h^0A^0Z^0}$ and should thus be thoroughly invegtigated. The next-to-leading order (NLO) QCD corrections to neutral Higgs-boson pair production at hadron colliders were calculated in Refs. [4, 8], which showed that the QCD corrections can enhance the cross section of h^0A^0 production by approximately 30%.

Fixed-order perturbative predictions would be unreliable when the exponential enhancement from soft gluon dominates at the edge of the phase space. The large logarithms, such as $\alpha_s^n(M^2/p_T^2)\ln^m(M^2/p_T^2)$ at small p_T and $\alpha_s^n(1-z)^{-1}\ln^m(1-z)$ when $z=M^2/\hat{s}\to 1$, should be resummed in precision calculations. We extract such logarithms in the partonic matrix element by adopting the Collins-Soper-Sterman resummation technique [9-17] and analyze the threshold resummation effect from parton distribution functions (PDFs) by using the factorization method proposed in Ref. [18]. Generally, the resummation corrections are only considered for fixing the unnatural behaviours in the small-p_T and threshold regions, while the fixed-order predictions are suitable for describing the kinematics far away from the edge of the final-state phase space. Thus, the resummation results should be matched with the fixed-order predictions to obtain a reliable description in all kinematical regions.

In this study, we thoroughly analyze scalar-pseudoscalar pair production at the 13 TeV LHC within the type-I 2HDM at the NLO and next-to-leading logarithmic (NLL) accuracy in QCD. The rest of this paper is organized as follows. In Sec. II, we briefly review the 2HDM. In Sec. III, we present the calculation strategies for ϕ^0A^0 associated production at QCD NLO+NLL accuracy, including the Collins-Soper-Sterman resummation technique and the factorization method for assessing the impact of the threshold-resummation improved PDFs. The numerical results and discussion for both the integrated cross section and the differential distributions with respect to the transverse momentum and invariant mass of the final-state ϕ^0A^0 system are provided in Sec. IV. Finally, a short summary is given in Sec. V.

II. BRIEF REVIEW OF 2HDM

In contrast to the SM, the Higgs sector of the 2HDM consists of two complex scalar $SU(2)_{\rm L}$ doublets $\Phi_{1,2}$ with hypercharge $Y=+1$. The most general scalar potential, which is invariant under the $SU(2)_{\rm L}\otimes U(1)_{\rm Y}$ electroweak gauge symmetry and a discrete Z_2 symmetry $\Phi_i \to (-1)^{i+1}\Phi_i$ ($i=1,2$), is given by

$$\begin{aligned} V(\Phi_1,\Phi_2) =& m_{11}^2\Phi_1^\dagger\Phi_1 + m_{22}^2\Phi_2^\dagger\Phi_2 - (m_{12}^2\Phi_1^\dagger\Phi_2 + \text{h.c.}) \\ &+ \frac{1}{2}\lambda_1(\Phi_1^\dagger\Phi_1)^2 + \frac{1}{2}\lambda_2(\Phi_2^\dagger\Phi_2)^2 \\ &+ \lambda_3(\Phi_1^\dagger\Phi_1)(\Phi_2^\dagger\Phi_2) + \lambda_4(\Phi_1^\dagger\Phi_2)(\Phi_2^\dagger\Phi_1) \\ &+ \frac{1}{2}\left[\lambda_5(\Phi_1^\dagger\Phi_2)^2 + \text{h.c.}\right], \end{aligned} \tag{1}$$

where the dimension-two term m_{12}^2 is tolerated because it only breaks the Z_2 symmetry softly, and $m_{11,22}^2$, $\lambda_{1,2,3,4}$ are forced to be real owing to the hermiticity of the scalar potential. The two Higgs doublets can be parameterized as [3]

$$\Phi_i = \begin{pmatrix} \phi_i^+ \\ (v_i+\rho_i+i\eta_i)/\sqrt{2} \end{pmatrix} \qquad (i=1,2), \tag{2}$$

where v_1 and v_2 are the vacuum expectation values (VEVs) of the neutral components of Φ_1 and Φ_2, respectively. In a $\mathcal{CP}$-conserving 2HDM, both m_{12}^2 and λ_5 are real, and so are v_1 and v_2. The eight mass eigenstates of the Higgs sector are given by

$$\begin{pmatrix} H^0 \\ h^0 \end{pmatrix} = \begin{pmatrix} \cos\alpha & \sin\alpha \\ -\sin\alpha & \cos\alpha \end{pmatrix}\begin{pmatrix} \rho_1 \\ \rho_2 \end{pmatrix}, \tag{3}$$

$$\begin{pmatrix} G^0 \\ A^0 \end{pmatrix} = \begin{pmatrix} \cos\beta & \sin\beta \\ -\sin\beta & \cos\beta \end{pmatrix}\begin{pmatrix} \eta_1 \\ \eta_2 \end{pmatrix}, \tag{4}$$

$$\begin{pmatrix} G^\pm \\ H^\pm \end{pmatrix} = \begin{pmatrix} \cos\beta & \sin\beta \\ -\sin\beta & \cos\beta \end{pmatrix}\begin{pmatrix} \phi_1^\pm \\ \phi_2^\pm \end{pmatrix}, \tag{5}$$

where α is the mixing angle in the $\mathcal{CP}$-even Higgs sector and $\beta=\arctan\dfrac{v_2}{v_1}$ describes the mixing in the $\mathcal{CP}$-odd and charged Higgs sectors. After the spontaneous electroweak symmetry breaking, three out of eight degrees of freedom from $\Phi_{1,2}$ that correspond to Nambu-Goldstone bosons $G^\pm$and G^0 are respectively absorbed by weak gauge bosons $W^\pm$ and Z^0, providing the longitudinal polarizations of $W^\pm$ and Z^0. The remaining five degrees of freedom become the aforementioned five physical Higgs bosons: two $\mathcal{CP}$-even Higgs bosons h^0 and H^0, one $\mathcal{CP}$-odd Higgs boson A^0, and a pair of charged Higgs bosons $H^\pm$. In this study, the seven input parameters for the Higgs sector of a $\mathcal{CP}$-conserving 2HDM are chosen as

$$\left\{m_{h^0}, m_{H^0}, m_{A^0}, m_{H^\pm}, m_{12}^2, \sin(\beta-\alpha), \tan\beta\right\}, \tag{6}$$

which are implemented as the "physical basis" in *2HDMC* [19]. Then, the Higgs potential in Eq. (1) can be completely determined by the seven Higgs parameters in Eq. (6) and v, where $v\equiv\sqrt{v_1^2+v_2^2}=(\sqrt{2}G_{\rm F})^{-1/2}\approx 246$ GeV

has been classified as an electroweak input parameter.

To guarantee the absence of Higgs-mediated flavor changing neutral currents at the tree level, the Z_2 symmetry should be extended to the Yukawa sector. Given that the two Higgs doublets $\Phi_{1,2}$ have opposite Z_2 charges, each flavor of quark/lepton can only couple to one of the two Higgs doublets. There are four allowed types of Yukawa interaction corresponding to the four independent Z_2 charge assignments on the quark and lepton $SU(2)_{\rm L}$ multiplets (Table 1). The Yukawa Lagrangian of the 2HDM can be expressed in terms of Higgs mass eigenstates as

$$\begin{aligned}\mathcal{L}^{\rm 2HDM}_{\rm Yukawa} =& -\sum_{f=u,d,\ell}\frac{m_f}{v}\left(\xi^f_h\bar{f}fh^0+\xi^f_H\bar{f}fH^0-{\rm i}\xi^f_A\bar{f}\gamma^5fA^0\right)\\ &-\left[\frac{\sqrt{2}V_{ud}}{v}\bar{u}\left(m_u\xi^u_AP_{\rm L}+m_d\xi^d_AP_{\rm R}\right)dH^+\right.\\ &\left.+\frac{\sqrt{2}m_\ell}{v}\xi^\ell_A\bar{\nu}P_{\rm R}\ell H^+ +{\rm h.c.}\right],\end{aligned}\tag{7}$$

where $\xi^f_{h,H,A}$ $(f=u,d,\ell)$ are the Higgs Yukawa couplings normalized to the SM vertices, and the corresponding values in the type-I, type-II, lepton-specific, and flipped 2HDMs are listed in Table 2.

The Higgs gauge interaction is independent of the types of the 2HDM. The couplings of h^0 and H^0 to weak gauge boson pair are proportional to $\sin(\beta-\alpha)$ and $\cos(\beta-\alpha)$, respectively. The 2HDM parameter space is stringently constrained by the requirement that one out of the two neutral $\mathcal{CP}$-even Higgs bosons has physical properties consistent with the 125 GeV scalar discovered at the CERN LHC. It is well known that if one of the two neutral $\mathcal{CP}$-even Higgs mass eigenstates is approximately aligned in the two-dimensional Higgs field space with the direction of the Higgs VEV vector $\vec{v}\equiv(v_1,v_2)$ (the so-called alignment limit), the couplings of this Higgs boson are SM-like. The two alignment limits of the 2HDM are listed in Table 3. Given that the SM-like Higgs boson with mass around 125 GeV seems to be favored by LHC data, we will investigate the scalar-pseudoscalar pair production at the LHC only at the alignment limit.

Table 1. Four types of 2HDMs and the corresponding Z_2 charge assignments on Higgs, quark, and lepton $SU(2)_{\rm L}$ multiplets.

2HDM	Φ_1	Φ_2	$Q_{\rm L}$	$L_{\rm L}$	$u_{\rm R}$	$d_{\rm R}$	$\ell_{\rm R}$
Type I	+	−	+	+	−	−	−
Type II	+	−	+	+	−	+	+
Lepton-specific	+	−	+	+	−	−	+
Flipped	+	−	+	+	−	+	−

Table 2. Normalized Higgs Yukawa couplings $\xi^f_{h,H,A}$ $(f=u,d,\ell)$ in the type-I, type-II, lepton-specific, and flipped 2HDMs. $(\tilde{\alpha},\tilde{\beta})=(\alpha,\beta)+\frac{\pi}{2}$.

2HDM	Type I	Type II	Lepton-specific	Flipped
ξ^u_h	$\cos\alpha/\sin\beta$			
ξ^u_H	$\sin\alpha/\sin\beta$	√		√
ξ^u_A	$\cot\beta$		√	
ξ^d_h	$\cos\alpha/\sin\beta$			
ξ^d_H	$\sin\alpha/\sin\beta$			$(\alpha,\beta)\to(\tilde{\alpha},\tilde{\beta})$
ξ^d_A	$-\cot\beta$	$(\alpha,\beta)\to(\tilde{\alpha},\tilde{\beta})$		
ξ^ℓ_h	$\cos\alpha/\sin\beta$			
ξ^ℓ_H	$\sin\alpha/\sin\beta$		$(\alpha,\beta)\to(\tilde{\alpha},\tilde{\beta})$	√
ξ^ℓ_A	$-\cot\beta$			

Table 3. Two alignment limits of the 2HDM.

Alignment limit	$\beta-\alpha$	h^0	H^0
I	$\pi/2$	SM-like	
II	0		SM-like

III. CALCULATION STRATEGY

We adopt the 't Hooft-Feynman gauge and take the five-flavor scheme in our calculations. Apart from the top quark, all other light quarks, including the bottom quark, are treated as massless particles. The UV and IR divergences in the QCD loop and real jet emission corrections are regularized by adopting the dimensional regularization scheme [20]. We employ both the Catani-Seymour dipole subtraction method [21, 22] and the two cutoff phase space slicing method [23] to separate the soft and collinear IR singularities of the real emission correction, and then cross check their correctness.

A. Electroweak production via quark-antiquark annihilation

The scalar-pseudoscalar pair can be produced at the LHC via Drell-Yan production mechanism. Some representative LO and QCD NLO Feynman diagrams for $q\bar{q}\to H^0(h^0)A^0$ are shown in Fig. 1 . In this study, we categorize $qg\to H^0(h^0)A^0+q$ as the real light-quark emission correction to the quark-antiquark-initiated Drell-Yan channel.

The $h^0A^0Z^0$ and $H^0A^0Z^0$ gauge interactions in the 2HDM are given by

$$\begin{aligned}g_{h^0A^0Z^0}&=\frac{e\cos(\beta-\alpha)}{\sin2\theta_{\rm W}}(p_{h^0}-p_{A^0})_\mu,\\ g_{H^0A^0Z^0}&=-\frac{e\sin(\beta-\alpha)}{\sin2\theta_{\rm W}}(p_{H^0}-p_{A^0})_\mu,\end{aligned}\tag{8}$$

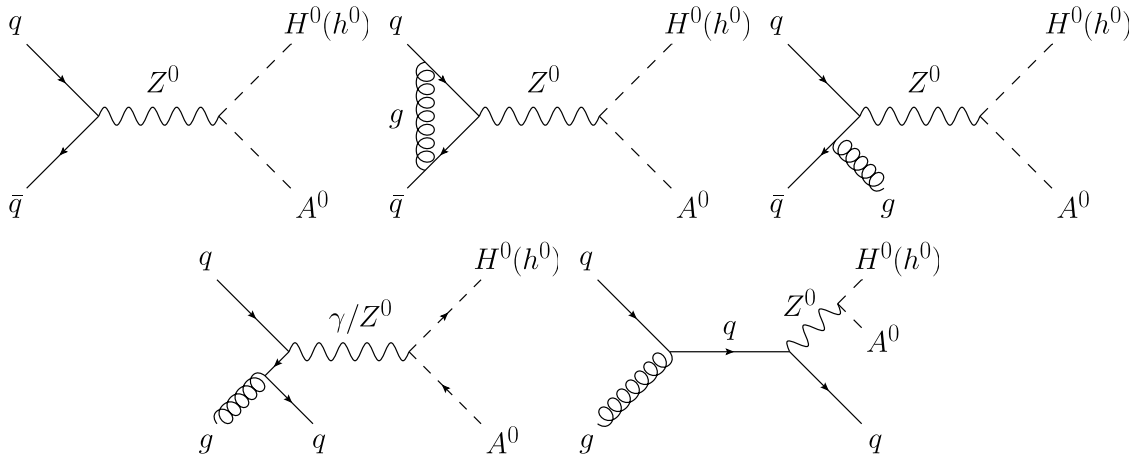

Fig. 1. Representative LO and QCD NLO Feynman diagrams for $q\bar{q} \to H^0(h^0)A^0$.

where $\theta_{\rm W}$ is the Weinberg weak mixing angle, p_{h^0,H^0,A^0} are the incoming momenta of the corresponding (pseudo)scalars, and μ is the Lorentz index of the vector boson Z^0. At the alignment limit, one of the two $C\!P$-even mass eigenstates can be regarded as the SM Higgs boson $h^0_{\rm SM}$, while the other is a BSM $C\!P$-even Higgs boson denoted by ϕ^0. We can see from Table 3 that

$$(h^0_{\rm SM},\phi^0) = \begin{cases} (h^0,H^0), & (\text{alignment limit I}: \ \sin(\beta-\alpha)=1), \\ (H^0,h^0), & (\text{alignment limit II}: \ \cos(\beta-\alpha)=1). \end{cases} \tag{9}$$

Given that the $h^0A^0Z^0$ and $H^0A^0Z^0$ coupling strengths are proportional to $\cos(\beta-\alpha)$ and $\sin(\beta-\alpha)$, respectively, the $h^0_{\rm SM}A^0$ associated production is forbidden up to $O(\alpha^2\alpha_s)$ at the alignment limit. Thus, we only focus on the Drell-Yan production of ϕ^0A^0 in the following.

The doubly-differential cross section for $pp \to \phi^0A^0+X$ can be perturbatively calculated by means of the QCD factorization theorem:

$$\begin{aligned} M^2\frac{{\rm d}^2\sigma}{{\rm d}M^2{\rm d}p_T^2}(\tau) = \sum_{a,b}\int_0^1 {\rm d}x_a{\rm d}x_b{\rm d}z\Big[x_af_{a/P}(x_a,\mu_F^2)\Big] \\ \times\Big[x_bf_{b/P}(x_b,\mu_F^2)\Big] \\ \times\Big[z\hat{\sigma}_{ab}(z,M^2,p_T^2,\mu_F^2,\mu_R^2)\Big] \\ \times\delta(\tau-x_ax_bz), \end{aligned} \tag{10}$$

where M and p_T are the invariant mass and transverse momentum of the final-state ϕ^0A^0 system, respectively. The threshold variables τ and z in Eq. (10) are defined by

$$\tau = (M/\sqrt{s})^2, \quad z = (M/\sqrt{\hat{s}})^2, \tag{11}$$

where $\sqrt{s}$ and $\sqrt{\hat{s}}$ denote the hadronic and partonic center-of-mass energies, respectively. The universal PDF $f_{a/P}(x,\mu_F^2)$ gives the probability to find parton a in proton P at factorization scale μ_F as a function of fraction x of the proton's longitudinal momentum carried by the parton. After preforming a Mellin transformation,

$$F(N) = \int_0^1 {\rm d}y y^{N-1}F(y), \tag{12}$$

on Eq. (10), the hadronic cross section can be written as a simple product of the PDFs and the partonic cross section in the conjugate Mellin N-space as

$$\begin{aligned} M^2\frac{{\rm d}^2\sigma}{{\rm d}M^2{\rm d}p_T^2}(N-1) = \sum_{a,b}f_{a/P}(N,\mu_F^2)f_{b/P}(N,\mu_F^2) \\ \times\hat{\sigma}_{ab}(N,M^2,p_T^2,\mu_F^2,\mu_R^2). \end{aligned} \tag{13}$$

To be consistent with the CT collaboration [24], we refit the PDF, $f_{a/P}(x,\mu_F^2)$, as a polynomial of $x^{1/2}$ with eight coefficients,

$$\begin{aligned} f_{a/P}(x,\mu_F^2) = A_0x^{A_1}(1-x)^{A_2}\Big(1+A_3x^{1/2}+A_4x \\ +A_5x^{3/2}+A_6x^2+A_7x^{5/2}\Big). \end{aligned} \tag{14}$$

Thus, the Mellin moment of the PDF has the form

$$\begin{aligned} f_{a/P}(N,\mu_F) = A_0\Big[{\rm B}(A_1+N,A_2+1)+A_3{\rm B}(A_1+N+1/2,A_2+1) \\ +A_4{\rm B}(A_1+N+1,A_2+1)+A_5{\rm B}(A_1+N+3/2,A_2+1) \\ +A_6{\rm B}(A_1+N+2,A_2+1)+A_7{\rm B}(A_1+N+5/2,A_2+1)\Big], \end{aligned} \tag{15}$$

where $\mathrm{B}(x,y)\equiv\Gamma(x)\Gamma(y)/\Gamma(x+y)$ is the Beta function.

According to the factorization scheme presented in Ref. [25], the partonic cross section can be expressed as a product of a process-dependent hard function and a process-independent Sudakov exponential term [13, 14, 26-29]. The higher-order QCD contributions to the partonic cross section contain logarithmic terms of type $\alpha_s^n(M^2/p_T^2)\ln^m(M^2/p_T^2)$, which become large in the small-p_T region. These logarithmically-enhanced contributions arising at small p_T spoil the convergence of the fixed-order perturbative expansion and must therefore be resummed to all orders in α_s. We adopt the b-space resummation approach, which was fully formulated by Collins, Soper, and Sterman [9-12], to systematically resum the large logarithmic terms at small p_T. In this approach, a Bessel transform is applied to the partonic cross section,

$$\hat{\sigma}_{ab}(N,M^2,p_T^2,\mu_F^2,\mu_R^2)=\int_0^\infty \mathrm{d}b\frac{b}{2}J_0(bp_T)\times\hat{\sigma}_{ab}(N,M^2,b^2,\mu_F^2,\mu_R^2),\quad(16)$$

where $J_0(x)$ is the zeroth-order Bessel function. Given that impact parameter b is the variable conjugate to transverse momentum p_T, the limit $M/p_T\to 0$ corresponds to $Mb\to\infty$. Therefore, the large logarithms of M/p_T arising at small p_T turn into large logarithms of Mb,

$$\left[(M^2/p_T^2)\ln^m(M^2/p_T^2)\right]_+\longrightarrow\ln^{m+1}(M^2b^2)+\cdots\quad(17)$$

After performing the resummation procedure, the resummed partonic cross section in the conjugate b-space at the NLL accuracy can be expressed as [9-12]

$$\hat{\sigma}_{ab}^{(\mathrm{res.})}(N,M^2,b^2,\mu_F^2,\mu_R^2)=\sum_{a',a'',b',b''}E_{a'a}^{(1)}(N,1/\bar{b}^2,\mu_F^2)\times E_{b'b}^{(1)}(N,1/\bar{b}^2,\mu_F^2)\mathcal{C}_{a''a'}(N,1/\bar{b}^2)\times\mathcal{C}_{b''b'}(N,1/\bar{b}^2)\mathcal{H}_{a''b''}(M^2,\mu_R^2)\times\exp\left[\mathcal{G}_{a''b''}(M^2\bar{b}^2,M^2,\mu_R^2)\right],\quad(18)$$

where $\bar{b}$ is the normalized impact parameter defined by $\bar{b}=b/b_0$ with $b_0=2\mathrm{e}^{-\gamma_\mathrm{E}}$ [17], and the one-loop QCD evolution operator $E_{ab}^{(1)}$ is derived from the collinear-improved procedure as recommended in Refs. [30-34]. In the physical resummation scheme, the coefficient function $\mathcal{C}_{ab}$ and the Sudakov form factor $\mathcal{G}_{ab}$ are free from any hard contributions, and the hard function $\mathcal{H}_{ab}$, determined by the finite part of the renormalized virtual contribution, is free from any logarithmic contributions [16]. To transform the resummed partonic cross section $\hat{\sigma}_{ab}^{(\mathrm{res.})}(N,M^2,b^2,\mu_F^2,\mu_R^2)$ back to the physical p_T-space, we rewrite Eq. (16) as [35]

$$\hat{\sigma}_{ab}^{(\mathrm{res.})}(N,M^2,p_T^2,\mu_F^2,\mu_R^2)=\sum_{k=1,2}\int_{C_k}\mathrm{d}b\frac{b}{4}h_k(bp_T,v)\times\hat{\sigma}_{ab}^{(\mathrm{res.})}(N,M^2,b^2,\mu_F^2,\mu_R^2),\quad(19)$$

where

$$h_k(x,v)=\frac{(-1)^k}{\pi}\int_{-iv\pi}^{(-1)^k\pi+iv\pi}\mathrm{d}\theta\mathrm{e}^{-\mathrm{i}x\sin\theta},\qquad(k=1,2),\quad(20)$$

are two auxiliary Hankel-like functions satisfying $h_1(x,v)+h_2(x,v)=2J_0(x)$, and the integration contours C_k $(k=1,2)$ in the complex b-plane are defined by

$$C_k:\quad b=b(t)\equiv t\mathrm{e}^{(-1)^k i\varphi},\qquad t\in[0,+\infty)\quad\text{with}\quad\varphi\in(0,\pi/2).\quad(21)$$

It is well known that such contours avoid the Landau pole by a deformation into either the upper or lower half complex b-plane.

The invariant mass distribution of the final-state ϕ^0A^0 system in the Mellin N-space can be obtained by integrating Eq. (13) over the transverse momentum p_T. In the threshold regime, the large logarithmic terms of the type $\alpha_s^n(1-z)^{-1}\ln^m(1-z)$ also spoil the convergence of the perturbative series. These singular terms turn into large logarithms of the Mellin variable, N:

$$\left[(1-z)^{-1}\ln^m(1-z)\right]_+\longrightarrow\ln^{m+1}N+\cdots.\quad(22)$$

The corresponding resummed partonic cross section for invariant mass distribution at the NLL accuracy can be expressed as [36, 37]

$$\hat{\sigma}_{ab}^{(\mathrm{res.})}(N,M^2,\mu_F^2,\mu_R^2)=\sum_{a',b'}E_{a'a}^{(1)}(N,M^2/\bar{N}^2,\mu_F^2)\times E_{b'b}^{(1)}(N,M^2/\bar{N}^2,\mu_F^2)\tilde{\mathcal{H}}_{a'b'}(M^2,\mu_R^2)\times\exp\left[\tilde{\mathcal{G}}_{a'b'}(\bar{N},M^2,\mu_R^2)\right],\quad(23)$$

where $\bar{N}$ is the reduced Mellin variable defined by $\bar{N}=N\mathrm{e}^{\gamma_\mathrm{E}}$.

The hard functions, $\mathcal{H}_{ab}$ and $\tilde{\mathcal{H}}_{ab}$, do not contain any large logarithms. They can be perturbatively calculated and read at the NLO accuracy:

$$\mathcal{H}_{ab}(M^2,\mu_R^2) = \hat{\sigma}_{ab}^{(0)}(M^2)(1+a_s\mathcal{A}_0),$$
$$\tilde{\mathcal{H}}_{ab}(M^2,\mu_R^2) = \mathcal{H}_{ab}(M^2,\mu_R^2) + a_s\frac{\pi^2}{6}\left[A_a^{(1)}+A_b^{(1)}\right]\hat{\sigma}_{ab}^{(0)}(M^2), \tag{24}$$

where $a_s = \alpha_s/(2\pi)$, $A_a^{(1)} = 2C_a$ [1)], $\hat{\sigma}_{ab}^{(0)}$ is the lowest-order partonic cross section, and $\mathcal{A}_0$ represents the IR-finite part of the renormalized virtual correction in the dimensional regularization scheme, i.e.,

$$\hat{\sigma}_{ab}^{(\text{vir.})}(M^2,\mu_R^2) = a_s\left(\frac{4\pi\mu_R^2}{M^2}\right)^{\epsilon}\frac{\Gamma(1-\epsilon)}{\Gamma(1-2\epsilon)}\left(\frac{\mathcal{A}_{-2}}{\epsilon^2} + \frac{\mathcal{A}_{-1}}{\epsilon} + \mathcal{A}_0\right)\hat{\sigma}_{ab}^{(0)}(M^2) + O(\epsilon). \tag{25}$$

The Sudakov form factors $\mathcal{G}_{ab}$ and $\tilde{\mathcal{G}}_{ab}$ collect all the logarithmically-enhanced contributions and take the form

$$\mathbb{G}_{ab}(\omega,M^2,\mu_R^2) = L\mathbb{G}_{ab}^{(1)}(\lambda) + \sum_{n=0}^{+\infty} a_s^n\mathbb{G}_{ab}^{(n+2)}(\lambda,M^2/\mu_R^2),$$
$$(\mathbb{G} = \mathcal{G} \text{ or } \tilde{\mathcal{G}}), \tag{26}$$

with $\lambda = a_s\beta_0 L$, $L = \ln\omega$, and $\omega = M^2\bar{b}^2$ and $\bar{N}$ for $\mathbb{G} = \mathcal{G}$ and $\tilde{\mathcal{G}}$, respectively. The function $\mathbb{G}_{ab}^{(n+1)}$ $(n = 0,1,2,...)$ on the right side of Eq. (26) resums all the N^{n}LL contributions. In this study, we only consider the LL and NLL terms, i.e., $L\mathbb{G}_{ab}^{(1)}$ and $\mathbb{G}_{ab}^{(2)}$, because the electroweak production of ϕ^0A^0 is studied at the NLO+NLL accuracy. The analytic expressions for $\mathbb{G}_{ab}^{(1)}$ and $\mathbb{G}_{ab}^{(2)}$ can be found in Ref. [38]. Finally, the C_{ab} function in Eq. (18) at the NLL accuracy can be expressed as

$$C_{ab}(N,\mu_R^2) = \delta_{ab} + a_s\left[\frac{\pi^2}{6}C_a\delta_{ab} - P'_{ab}(N)\right], \tag{27}$$

where $P'_{ab}(N)$ is the $O(\epsilon)$ part of the unregulated Altarelli-Parisi splitting function in the Mellin N-space, i.e.,

$$P_{ab}(z,\epsilon) = P_{ab}(z) + \epsilon P'_{ab}(z),$$
$$P'_{ab}(N) = \int_0^1 \mathrm{d}z z^{N-1}P'_{ab}(z). \tag{28}$$

The resummed partonic cross section $\hat{\sigma}_{ab}^{(\text{res.})}$ gives the dominant contribution in the small-p_T and threshold regions, while the fixed-order partonic cross section $\hat{\sigma}_{ab}^{(\text{f.o.})}$ dominates at large p_T and small $M/\sqrt{\hat{s}}$. To obtain a reliable theoretical prediction with uniform accuracy in all kinematical regions, the resummed and fixed-order results should be combined consistently by subtracting their overlap,

$$\hat{\sigma}_{ab} = \hat{\sigma}_{ab}^{(\text{res.})} + \hat{\sigma}_{ab}^{(\text{f.o.})} - \hat{\sigma}_{ab}^{(\text{o.l.})}. \tag{29}$$

This matching procedure guarantees that the combined result $\hat{\sigma}_{ab}$ contains both the perturbative contributions up to the specific fixed order and the logarithmically-enhanced contributions from higher orders. At the NLO+NLL accuracy, $\hat{\sigma}_{ab}^{(\text{o.l.})}$ in Eq. (29) can be obtained by expanding the resummed partonic cross section $\hat{\sigma}_{ab}^{(\text{res.})}$ to $O(\alpha_s)$, i.e.,

$$\hat{\sigma}_{ab}^{(\text{o.l.})} = \hat{\sigma}_{ab}^{(\text{res.})}(\alpha_s = 0) + \alpha_s\frac{\mathrm{d}\hat{\sigma}_{ab}^{(\text{res.})}}{\mathrm{d}\alpha_s}(\alpha_s = 0). \tag{30}$$

After multiplying the Mellin moments of the PDFs to the NLO+NLL matched partonic cross section $\hat{\sigma}_{ab}$, we obtain the hadronic differential cross section in the Mellin N-space. To get back to the physical space, an inverse Mellin transform,

$$F(\tau) = \frac{1}{2\pi i}\int_{C_N}\mathrm{d}N\tau^{-N}F(N), \tag{31}$$

should be applied to the right side of Eq. (13). To achieve this, we must comprehensively estimate the singularities in the Mellin N-space and choose an appropriate integration contour C_N. There are two types of singularities for the hadronic differential cross section in the Mellin N-space: (1) the poles in the Mellin moments of the PDFs (Regge poles), and (2) the Landau pole related to the running of the strong coupling constant. The integration contour C_N in the complex N-plane is chosen as [15]

$$C_N: \quad N = N(y) \equiv C + y\mathrm{e}^{\pm i\phi}, \qquad y \in [0,+\infty) \tag{32}$$

where $\phi \in [\pi/2,\pi)$ and the constant C is chosen such that the Regge and Landau poles lie to the left and right of C_N, respectively.

In principle, for NLO+NLL calculations, we should employ resummation-improved PDFs for initial-state parton convolution. The threshold-resummation improved PDFs are now available with the NNPDF3.0 set. Compared to the NNPDF3.0 global fit, the threshold-resummation improved PDF fit has to be performed with a reduced data set involving deep-inelastic scattering, Drell-Yan, and top-pair production data, because the threshold resummation calculations are not readily available for all the processes employed in the global analysis. The reduced data set used in the fit of the threshold-resumma-

1) $C_q = C_F = 4/3$ and $C_g = C_A = 3$.

tion improved PDF set would induce a relatively larger PDF error compared to the global PDF set. In this study, we adopt the factorization method proposed in Ref. [18] to combine the smaller PDF error of the global PDF set with the resummation effect from the threshold-resummation improved PDF set. In the factorization method, the NLO+NLL QCD corrected cross section can be approximately calculated by

$$\sigma^{\rm NLO+NLL} = K \times \sigma^{\rm NLO}\big|_{\rm (NLO\ global)}, \tag{33}$$

where

$$K = K_{\rm PDF} \times K_{\rm PME}, \tag{34}$$

$$K_{\rm PDF} = \frac{\sigma^{\rm NLO+NLL}\big|_{\rm (NLO+NLL\ reduced)}}{\sigma^{\rm NLO+NLL}\big|_{\rm (NLO\ reduced)}},$$
$$K_{\rm PME} = \frac{\sigma^{\rm NLO+NLL}\big|_{\rm (NLO\ global)}}{\sigma^{\rm NLO}\big|_{\rm (NLO\ global)}} \tag{35}$$

which describe the impact of the threshold-resummation improved PDFs and the NLL resummation effect from the partonic matrix element, respectively. Subscripts "NLO+NLL reduced " and "NLO reduced " appearing in the definition of $K_{\rm PDF}$ denote the threshold-resummation improved PDF set NNPDF30_nll_disdytop and its fixed-order version NNPDF30_nlo_disdytop [39], respectively. It is well known that the NNPDF cannot be properly transformed to the Mellin space; the refit of the NNPDF replicas in the Mellin space would lead to some convergence issues [40]. Fortunately, however, $K_{\rm PME}$ is expected to be largely independent of the PDF choice because the PDF sets used in $K_{\rm PME}$ are estimated at the same perturbative order [40]. This feature has been verified with the CT18NLO and MSTW2008nlo68cl PDFs, and thus we choose CT18NLO as the "NLO global" PDF set in our calculations.

B. QCD production via gluon-gluon fusion

Compared to the electroweak production via quark-antiquark annihilation, the gluon-initiated QCD production of the scalar-pseudoscalar pair is a loop-induced production channel. This production mechanism should be taken into consideration at the LHC due to the high luminosity of gluon in proton. In Fig. 2 we depict some representative Feynman diagrams for $gg \to \phi^0 A^0$ at the lowest order. Note that the production rate relies not only on the heavy-quark Yukawa couplings, but also on the triple Higgs self-couplings. Unlike the quark-antiquark annihilation channel, the loop-induced gluon-gluon fusion channel is extremely sensitive to the Yukwawa interaction of the 2HDM. Due to the introduction of a soft breaking Z_2 symmetry to avoid tree-level FCNCs, each fermion type is only able to couple to one of the two Higgs doublets. There are four allowed types of 2HDMs, type-I, type-II, lepton-specific, and flipped, which correspond to the four different types of Yukawa interaction. In this study, we mainly focused on the type-I 2HDM and calculated the gluon-gluon fusion channel by using the modified *FeynArts-3.9*, *FormCalc-7.3*, and *LoopTools-2.8* packages [41-43].

IV. NUMERICAL RESULTS AND DISCUSSION

In this section, we provide some numerical results for $pp \to \phi^0 A^0 + X$ at the 13 TeV LHC in the type-I 2HDM. The SM input parameters used in this study are set as [44]

$$m_W = 80.379\ {\rm GeV},\ m_Z = 91.1876\ {\rm GeV},\ m_t = 172.76\ {\rm GeV},$$
$$G_{\rm F} = 1.1663787 \times 10^{-5}\ {\rm GeV}^{-2},\quad \alpha_s(m_Z) = 0.118. \tag{36}$$

The input parameters for the Higgs sector of the 2HDM should satisfy the theoretical constraints from perturbative unitarity [45], stability of vacuum [46], and tree-level unitarity [47], which can be checked by 2HDMC [19]. Moreover, the high-energy experiments can also give stringent constraints on the 2HDM input parameters. One of the experimental limits is that the partial width of $Z^0 \to H^0 A^0 / h^0 A^0$ cannot exceed 2σ uncertainty of the Z-width measurement [44], and others come from the restriction of the physical observables of B meson decays, the measurement of the SM-like Higgs property, and the direct search of Higgs state at the LEP, Tevatron, and LHC, which are integrated in the *SuperIso* [48], *HiggsSignals* [49], and *Higgsbounds* [50] packages, respectively.

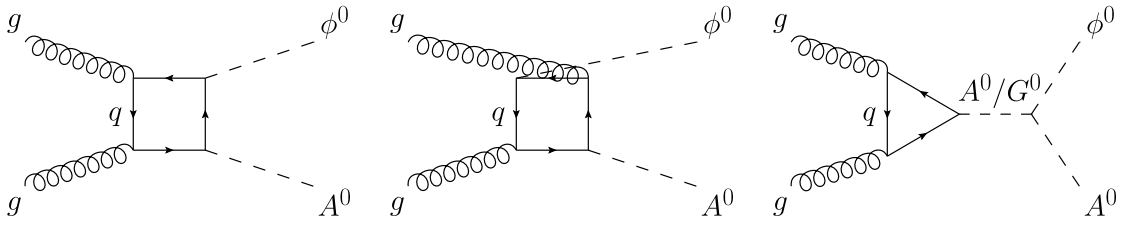

Fig. 2. Representative Feynman diagrams for $gg \to \phi^0 A^0$ at the lowest order.

We use the CT14lo PDF set [24] to perform LO calculation, and employ the CT18NLO PDF [51] to obtain NLO and NLO+NLL QCD corrected cross sections. CT18NLO PDF contains 1 central PDF set and 2×29 Hessian replicas. The PDF uncertainties of a cross section σ calculated with the CT18NLO PDF are given by [52]

$$\delta^{+}_{\rm PDF} = \frac{1}{\sigma_0}\sqrt{\sum_{i=1}^{29}\left[\max\{\sigma_{i+}-\sigma_0,\sigma_{i-}-\sigma_0,0\}\right]^2},$$
$$\delta^{-}_{\rm PDF} = \frac{1}{\sigma_0}\sqrt{\sum_{i=1}^{29}\left[\max\{\sigma_0-\sigma_{i+},\sigma_0-\sigma_{i-},0\}\right]^2}, \quad (37)$$

where σ_0 is the central value calculated with central set and $\sigma_{i\pm}$ $(i=1,...,29)$ are the cross sections evaluated with replicas. The factorization scale μ_F and the renormalization scale μ_R are set to be equal, i.e., $\mu_F=\mu_R=\mu$, for simplicity. The scale uncertainties of an integrated cross section σ are defined by

$$\delta^{+}_{\mu} = \frac{\max\{\sigma(\mu)\big|\mu_0/2\leqslant\mu\leqslant2\mu_0\}-\sigma(\mu_0)}{\sigma(\mu_0)},$$
$$\delta^{-}_{\mu} = \frac{\min\{\sigma(\mu)\big|\mu_0/2\leqslant\mu\leqslant2\mu_0\}-\sigma(\mu_0)}{\sigma(\mu_0)}, \quad (38)$$

where μ_0 is the central scale. The total theoretical error is defined as the sum in quadrature of the PDF and scale uncertainties. For the quark-initiated Drell-Yan production channel, $pp\to q\bar{q}\to\phi^0A^0$, the production rate will be calculated at the NLO+NLL accuracy in QCD, and the NLO and NLO+NLL relative corrections are respectively defined as

$$\delta^{\rm NLO}=\frac{\sigma^{\rm NLO}-\sigma^{\rm LO}}{\sigma^{\rm LO}},\quad \delta^{\rm NLO+NLL}=\frac{\sigma^{\rm NLO+NLL}-\sigma^{\rm LO}}{\sigma^{\rm LO}}. \quad (39)$$

Regarding the gluon-gluon fusion channel, $pp\to gg\to\phi^0A^0$, we only consider the lowest-order contribution since it is a loop-induced channel.

A. Integrated cross section

In this subsection, we present the integrated cross sections for ϕ^0A^0 associated production at $\sqrt{s}=13$ TeV LHC at the alignment limit in the 2HDM. The masses of ϕ^0 and A^0 can be alternatively described by the following three parameters,

$$m=\min\left(m_{\phi^0},m_{A^0}\right),\qquad \Delta m=\left|m_{\phi^0}-m_{A^0}\right|,$$
$$\epsilon=\text{sign}\left(m_{\phi^0}-m_{A^0}\right), \quad (40)$$

i.e., the minimal mass and mass hierarchy of ϕ^0 and A^0. The two scenarios in which $\epsilon=+1$ $(m_{\phi^0}>m_{A^0})$ and $\epsilon=-1$ $(m_{\phi^0}<m_{A^0})$ may be referred to as the normal mass hierarchy and inverted mass hierarchy, respectively.

The Drell-Yan production channel depends only on the masses of ϕ^0 and A^0[1)]. Furthermore, its integrated cross section is independent of ϵ. In our calculations, we set 0, 50, and 100 GeV as three benchmark values of Δm, which correspond, respectively, to the following three ϕ^0-A^0 mass splitting scenarios:

- degenerate scenario: $\Delta m=0$
- hierarchical scenario with small mass splitting: $0<\Delta m<m_Z$
- hierarchical scenario with large mass splitting: $\Delta m>m_Z$

The LO, NLO, NLO+NLL QCD corrected integrated cross sections and the corresponding theoretical relative errors induced by the factorization/renormalization scale and PDFs for $pp\to q\bar{q}\to\phi^0A^0$ as functions of m for $\Delta m=0$, 50 and 100 GeV are given in Tables 4, 5, and 6, respectively. The central scale is set as $\mu_0=m_{\phi^0}+m_{A^0}$. There is no PDF-induced theoretical error for the LO cross section because the CT14lo PDF used in the LO calculation contains only one central set but no PDF replicas. To study the full NLL resummation effect and the impact of the threshold-resummation improved PDFs in our calculations, we also provide the factorization K-factors K and $K_{\rm PDF}$ in these tables. The NLO+NLL QCD relative correction $\delta^{\rm NLO+NLL}$ and the matrix-element-induced factorization K-factor $K_{\rm PME}$ can be straightforwardly calculated by using $\delta^{\rm NLO}$, K, and $K_{\rm PDF}$,

$$\delta^{\rm NLO+NLL}=(K-1)+K\delta^{\rm NLO},\qquad K_{\rm PME}=\frac{K}{K_{\rm PDF}}. \quad (41)$$

As shown in Tables 4, 5, and 6, the QCD correction can significantly enhance the LO production cross section, especially for light scalar-pseudoscalar pair. The NLO QCD relative correction exceeds 30% at $m=50$ GeV, and decreases gradually to approximately 5.9%, 5.3%, and 4.8% for $\Delta m=0$, 50, and 100 GeV, respectively, as m increases to 800 GeV. The full NLL resummation correction (quantitatively described by $K-1$) slightly enhances the NLO QCD corrected cross section

1) $\sin(\beta-\alpha)$ has been fixed at the alignment limit.

Table 4. LO, NLO, NLO+NLL QCD corrected integrated cross sections, NLO QCD relative corrections, and factorization K-factors (K and $K_{\rm PDF}$) for $pp \to q\bar{q} \to \phi^0 A^0$ at $\sqrt{s} = 13$ TeV LHC within the 2HDM. The cross section central values are folded with the theoretical relative errors estimated from scale variation (first quote) and PDFs (second quote). The mass splitting between ϕ^0 and A^0 is fixed to zero ($\Delta m = 0$).

m[GeV]	$\sigma^{\rm LO}$[fb]	$\sigma^{\rm NLO}$[fb]	$\sigma^{\rm NLO+NLL}$[fb]	$\delta^{\rm NLO}$[%]	K	$K_{\rm PDF}$
50	$4923.7^{+8.5\%}_{-9.4\%}$	$6717.8^{+0.7\%+2.8\%}_{-0.4\%-3.7\%}$	$6731.0^{+0.0\%+2.8\%}_{-0.6\%-3.7\%}$	36.4	1.002	1.013
100	$218.7^{+2.5\%}_{-3.2\%}$	$290.2^{+0.9\%+2.9\%}_{-0.4\%-3.8\%}$	$290.8^{+0.0\%+2.9\%}_{-0.4\%-3.8\%}$	32.7	1.002	1.011
150	$49.41^{+0.1\%}_{-0.5\%}$	$63.75^{+1.4\%+3.3\%}_{-0.9\%-4.3\%}$	$63.94^{+0.0\%+3.3\%}_{-0.4\%-4.3\%}$	29.0	1.003	1.009
200	$16.98^{+1.2\%}_{-1.4\%}$	$21.40^{+1.6\%+3.6\%}_{-1.3\%-4.7\%}$	$21.49^{+0.1\%+3.6\%}_{-0.6\%-4.7\%}$	26.0	1.004	1.006
300	$3.504^{+3.4\%}_{-3.3\%}$	$4.249^{+1.9\%+4.3\%}_{-1.8\%-5.7\%}$	$4.267^{+0.8\%+4.3\%}_{-1.2\%-5.7\%}$	21.3	1.004	1.001
400	$1.051^{+4.9\%}_{-4.5\%}$	$1.233^{+2.2\%+5.0\%}_{-2.2\%-6.3\%}$	$1.237^{+1.5\%+5.0\%}_{-1.7\%-6.3\%}$	17.3	1.003	0.994
500	$0.3848^{+6.0\%}_{-5.4\%}$	$0.4387^{+2.4\%+5.8\%}_{-2.5\%-7.1\%}$	$0.4392^{+2.1\%+5.8\%}_{-2.2\%-7.1\%}$	14.0	1.001	0.985
600	$0.1597^{+6.9\%}_{-6.2\%}$	$0.1773^{+2.6\%+6.6\%}_{-2.8\%-7.9\%}$	$0.1771^{+2.6\%+6.6\%}_{-2.9\%-7.9\%}$	11.0	0.999	0.977
700	$0.07213^{+7.8\%}_{-6.9\%}$	$0.07818^{+2.8\%+7.5\%}_{-3.1\%-8.8\%}$	$0.07770^{+3.2\%+7.5\%}_{-3.5\%-8.8\%}$	8.39	0.994	0.966
800	$0.03465^{+8.5\%}_{-7.4\%}$	$0.03670^{+3.0\%+8.4\%}_{-3.3\%-9.7\%}$	$0.03618^{+3.7\%+8.4\%}_{-4.4\%-9.7\%}$	5.92	0.986	0.952

Table 5. Same as Table IV but for $\Delta m = 50$ GeV.

m [GeV]	$\sigma^{\rm LO}$ [fb]	$\sigma^{\rm NLO}$ [fb]	$\sigma^{\rm NLO+NLL}$ [fb]	$\delta^{\rm NLO}$ [%]	K	$K_{\rm PDF}$
50	$611.1^{+4.5\%}_{-5.3\%}$	$824.5^{+0.5\%+2.8\%}_{-0.0\%-3.7\%}$	$825.8^{+0.0\%+2.8\%}_{-0.4\%-3.7\%}$	34.9	1.002	1.012
100	$93.88^{+1.1\%}_{-1.6\%}$	$122.7^{+1.2\%+3.1\%}_{-0.7\%-4.0\%}$	$123.0^{+0.0\%+3.1\%}_{-0.3\%-4.0\%}$	30.7	1.002	1.010
150	$27.61^{+0.4\%}_{-0.7\%}$	$35.19^{+1.5\%+3.5\%}_{-1.1\%-4.5\%}$	$35.31^{+0.0\%+3.5\%}_{-0.5\%-4.5\%}$	27.5	1.003	1.007
200	$10.77^{+1.9\%}_{-2.0\%}$	$13.43^{+1.7\%+3.8\%}_{-1.4\%-4.9\%}$	$13.48^{+0.3\%+3.8\%}_{-0.8\%-4.9\%}$	24.7	1.004	1.005
300	$2.517^{+3.8\%}_{-3.6\%}$	$3.026^{+2.0\%+4.5\%}_{-1.9\%-5.8\%}$	$3.038^{+1.0\%+4.5\%}_{-1.3\%-5.8\%}$	20.2	1.004	0.999
400	$0.8032^{+5.2\%}_{-4.8\%}$	$0.9353^{+2.2\%+5.2\%}_{-2.3\%-6.5\%}$	$0.9388^{+1.6\%+5.2\%}_{-1.9\%-6.5\%}$	16.4	1.004	0.992
500	$0.3053^{+6.2\%}_{-5.6\%}$	$0.3457^{+2.4\%+6.0\%}_{-2.6\%-7.3\%}$	$0.3458^{+2.2\%+6.0\%}_{-2.5\%-7.3\%}$	13.2	1.000	0.983
600	$0.1299^{+7.2\%}_{-6.4\%}$	$0.1433^{+2.7\%+6.8\%}_{-2.8\%-8.1\%}$	$0.1430^{+2.8\%+6.8\%}_{-3.1\%-8.1\%}$	10.3	0.998	0.974
700	$0.05969^{+7.9\%}_{-7.0\%}$	$0.06432^{+2.9\%+7.7\%}_{-3.1\%-9.0\%}$	$0.06361^{+3.7\%+7.7\%}_{-3.3\%-9.0\%}$	7.76	0.989	0.960
800	$0.02904^{+8.6\%}_{-7.6\%}$	$0.03059^{+3.1\%+8.7\%}_{-3.4\%-9.9\%}$	$0.03008^{+3.9\%+8.7\%}_{-4.4\%-9.9\%}$	5.34	0.983	0.949

Table 6. Same as Table IV but for $\Delta m = 100$ GeV.

m[GeV]	$\sigma^{\rm LO}$[fb]	$\sigma^{\rm NLO}$[fb]	$\sigma^{\rm NLO+NLL}$[fb]	$\delta^{\rm NLO}$[%]	K	$K_{\rm PDF}$
50	$185.0^{+2.4\%}_{-3.0\%}$	$245.3^{+1.0\%+2.9\%}_{-0.4\%-3.9\%}$	$245.7^{+0.0\%+2.9\%}_{-0.4\%-3.9\%}$	32.6	1.002	1.011
100	$45.97^{+0.1\%}_{-0.4\%}$	$59.26^{+1.4\%+3.3\%}_{-1.0\%-4.3\%}$	$59.43^{+0.0\%+3.3\%}_{-0.4\%-4.3\%}$	28.9	1.003	1.009
150	$16.30^{+1.2\%}_{-1.4\%}$	$20.53^{+1.5\%+3.6\%}_{-1.4\%-4.8\%}$	$20.60^{+0.1\%+3.6\%}_{-0.7\%-4.8\%}$	26.0	1.003	1.006
200	$7.033^{+2.4\%}_{-2.5\%}$	$8.683^{+1.8\%+4.0\%}_{-1.6\%-5.2\%}$	$8.717^{+0.5\%+4.0\%}_{-0.9\%-5.2\%}$	23.5	1.004	1.004
300	$1.832^{+4.2\%}_{-3.9\%}$	$2.183^{+2.1\%+4.7\%}_{-2.0\%-5.9\%}$	$2.192^{+1.1\%+4.7\%}_{-1.5\%-5.9\%}$	19.2	1.004	0.998
400	$0.6183^{+5.5\%}_{-5.0\%}$	$0.7146^{+2.3\%+5.4\%}_{-2.3\%-6.7\%}$	$0.7168^{+1.8\%+5.4\%}_{-2.1\%-6.7\%}$	15.6	1.003	0.990
500	$0.2433^{+6.5\%}_{-5.8\%}$	$0.2736^{+2.5\%+6.2\%}_{-2.6\%-7.5\%}$	$0.2738^{+2.3\%+6.2\%}_{-2.7\%-7.5\%}$	12.5	1.001	0.982
600	$0.1059^{+7.4\%}_{-6.5\%}$	$0.1161^{+2.7\%+7.1\%}_{-2.9\%-8.4\%}$	$0.1157^{+2.9\%+7.1\%}_{-3.2\%-8.4\%}$	9.63	0.997	0.972
700	$0.04949^{+8.1\%}_{-7.2\%}$	$0.05301^{+2.9\%+7.9\%}_{-3.2\%-9.2\%}$	$0.05250^{+3.4\%+7.9\%}_{-3.8\%-9.2\%}$	7.11	0.990	0.959
800	$0.02438^{+8.8\%}_{-7.7\%}$	$0.02554^{+3.1\%+9.0\%}_{-3.4\%-10.1\%}$	$0.02505^{+3.9\%+9.0\%}_{-4.4\%-10.1\%}$	4.76	0.981	0.945

as $m < 500$ GeV, but suppresses it by approximately 2% in the high mass region. Compared to the full NLL resummation correction, the contribution from the threshold-resummation improved PDFs is more sensitive to m. The corresponding relative correction, i.e., $K_{\rm PDF}-1$, decreases monotonically as the increase of m, and reaches approximately -5% when $m = 800$ GeV. Moreover, we can find that the impact of the threshold-resummation improved PDFs becomes increasingly important with the increment of m for heavy scalar-pseudoscalar pair. On the contrary, the NLL QCD relative correction from the partonic matrix element, $K_{\rm PME}-1$, increases monotonically with the increment of m. It is almost independent of the mass splitting between ϕ^0 and A^0, varying from approximately -1% to 4% as m increases from 50 to 800 GeV.

The QCD production of ϕ^0A^0 via gluon-gluon fusion depends not only on m_{ϕ^0} and m_{A^0}, but also on m_{12}^2 and $\tan\beta$, since the Yukawa couplings and triple Higgs self-couplings are involved in this production channel. We calculate the lowest-order production cross section for this loop-induced channel at the two benchmark points listed in Table 7, which can satisfy both theoretical and experimental constraints. At both benchmark points, H^0 is the BSM $C\!P$-even Higgs boson, i.e., $H^0=\phi^0$, and $\sin(\beta-\alpha)=1$ at the alignment limit. The other two Higgs parameters of 2HDM, m_{h^0} and $m_{H^\pm}$, are not given in Table 7, because the scalar-pseudoscalar pair production at QCD NLO+NLL accuracy is completely independent from the SM-like and charged Higgs bosons. The integrated cross sections for $pp\to gg\to\phi^0A^0$ at $\sqrt{s}=13$ TeV LHC in the type-I 2HDM at BP1 and BP2, listed in Table 8, are approximately 1 and 0.06 fb, respectively. We can see that $\sigma_{gg}/\sigma^{\rm NLO+NLL}$, i.e., the ratio of the contribution from gluon-gluon fusion channel to the NLO+NLL QCD corrected cross section of quark-antiquark annihilation channel, is approximately 2.9% at BP1 and can reach 8.0% at BP2. It can be concluded that the scalar-pseudoscalar pair production at the LHC in the type-I 2HDM is predominated by the quark-initiated Drell-Yan production channel, and the gluon-gluon fusion contribution is non-negligible and should be taken into consideration in precision predictions.

Table 7. Benchmark points BP1 and BP2.

Benchmark point	m_{H^0}/GeV	m_{A^0}/GeV	m_{12}^2	$\tan\beta$
BP1	150	200	2000	10
BP2	400	500	50000	2

Table 8. Lowest-order integrated cross sections for $pp\to gg\to\phi^0A^0$ at $\sqrt{s}=13$ TeV LHC in type-I 2HDM at the benchmark points BP1 and BP2.

Benchmark point	BP1	BP2
σ_{gg}/fb	$1.020^{+26.4\%+3.7\%}_{-19.8\%-3.4\%}$	$0.05742^{+31.8\%+8.0\%}_{-22.7\%-6.4\%}$

B. Transverse momentum distribution

Next, we address the transverse momentum distribution of the scalar-pseudoscalar pair produced at the LHC. Since the one-loop-induced gluon-gluon fusion channel does not contribute to the p_T distribution due to the momentum conservation, we consider only the quark-initiated Drell-Yan production channel. The NLO, NLO+NLL QCD corrected transverse momentum distributions of ϕ^0A^0 as well as the overlap between the NLO QCD corrected and NLL QCD resummed p_T distributions (labeled by "NLO", "NLO+NLL", and "OVERLAP") for the Drell-Yan production of ϕ^0A^0 at $\sqrt{s}=13$ TeV LHC in the 2HDM at the benchmark points BP1 and BP2 are shown in Figs. 3(a) and 4(a), respectively. The central scale is $\mu_0=m_{\phi^0}+m_{A^0}$. As expected, the NLO QCD corrected p_T distribution and the overlap p_T distribution are in good agreement with each other in the small-p_T region [16] and become divergent as $p_T\to 0$, but the discrepancy between them becomes increasingly evident with the increment of p_T. The relative discrepancy between the NLO QCD corrected and the overlap p_T distributions, defined as

$$\eta=\left(\frac{{\rm d}\sigma^{\rm NLO}}{{\rm d}p_T}-\frac{{\rm d}\sigma^{\rm OVERLAP}}{{\rm d}p_T}\right)\Big/\frac{{\rm d}\sigma^{\rm NLO}}{{\rm d}p_T}\,, \tag{42}$$

can reach about 18.2% and 42.6% when $p_T=150$ and 300 GeV at BP1 and BP2, respectively. Compared to the NLO QCD corrected p_T distribution, the NLO+NLL QCD corrected p_T distribution is finite and more reliable in the whole final-state phase space. It increases sharply in the small-p_T region, reaches its maximum of around 1.9 fb/GeV in the vicinity of $p_T\sim 5.5$ GeV, and then decreases approximately logarithmically with the increment of p_T at the benchmark point BP1. Concerning the benchmark point BP2, the NLO+NLL QCD corrected p_T distribution peaks at $p_T\sim 7.5$ GeV and its maximum is approximately 0.027 fb/GeV.

The scale uncertainty of a differential distribution with respect to some kinematic variable x can be estimated by

$$\delta_\mu(x)=\max\left\{\frac{{\rm d}\sigma}{{\rm d}x}(\mu_1)-\frac{{\rm d}\sigma}{{\rm d}x}(\mu_2)\right\}\Big/\frac{{\rm d}\sigma}{{\rm d}x}(\mu_0)\,,$$
$$\mu_1,\mu_2\in[\mu_0/2,\,2\mu_0]\,. \tag{43}$$

In Figs. 3(b) and 4(b), we plot the scale uncertainties of the NLO and NLO+NLL QCD corrected p_T distributions, denoted by $\delta_\mu^{\rm NLO}$ and $\delta_\mu^{\rm NLO+NLL}$, at BP1 and BP2, respectively. As shown in the lower panels of Figs. 3(b) and 4(b), the scale uncertainty of the NLO QCD corrected p_T distribution increases gradually, while the scale

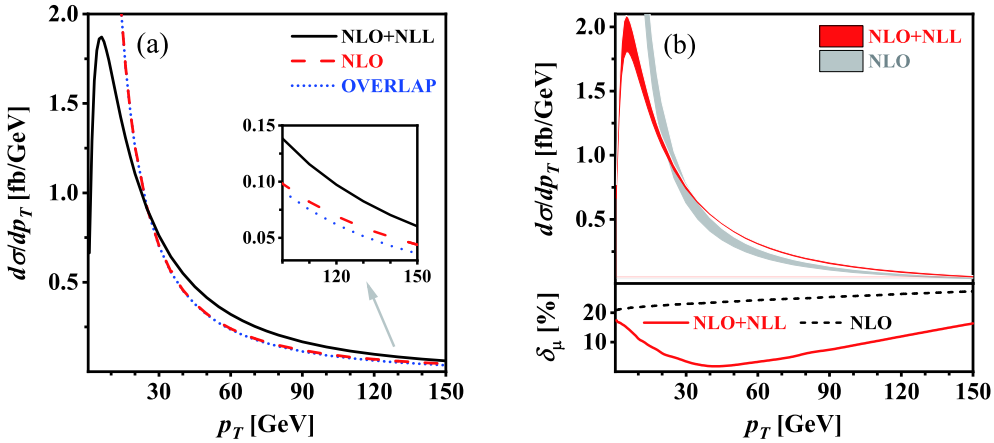

Fig. 3. (color online) (a) Transverse momentum distribution of final-state $\phi^0 A^0$ and (b) its scale uncertainty for $pp \to q\bar{q} \to \phi^0 A^0$ at $\sqrt{s} = 13$ TeV LHC within the 2HDM at the benchmark point BP1.

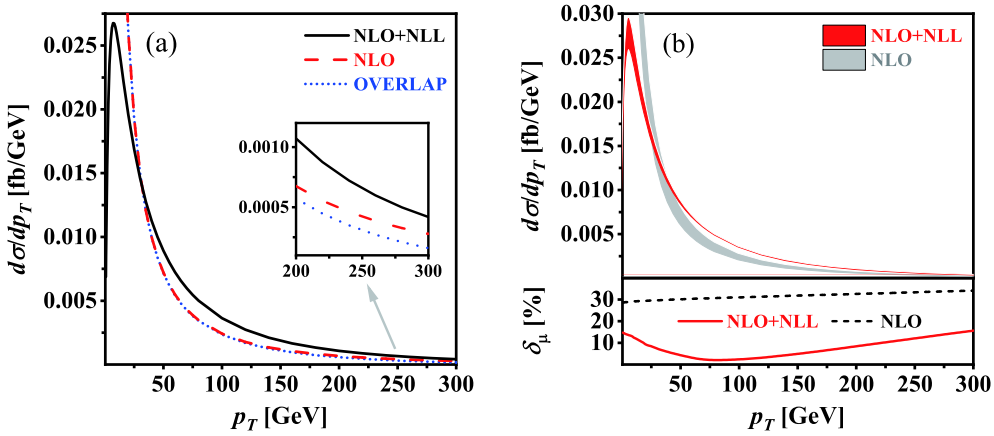

Fig. 4. (color online) Same as Fig. 3 but at BP2.

uncertainty of the NLO+NLL QCD corrected p_T distribution first decreases consistently before reaching its minimum and then increases monotonically, with the increment of p_T. Some representative values of $\delta_\mu^{\rm NLO}$ and $\delta_\mu^{\rm NLO+NLL}$ are given in Table 9. This table, as well as Figs. 3(b) and 4(b), clearly shows that $\delta_\mu^{\rm NLO+NLL}$ is much less than $\delta_\mu^{\rm NLO}$, especially in the intermediate-p_T region. Thus, we conclude that the resummation of higher-order large logarithmic contributions can significantly improve the fixed-order prediction for the p_T distribution; the NLO+NLL QCD corrected p_T distribution is much more reliable in the whole p_T region compared to the NLO QCD corrected p_T distribution.

Table 9. Scale uncertainties of NLO and NLO+NLL QCD corrected p_T distributions for $pp \to q\bar{q} \to \phi^0 A^0$ at $\sqrt{s} = 13$ TeV LHC within the 2HDM at BP1 and BP2 for some typical values of p_T.

Benchmark point	BP1		BP2	
	$p_T = 1$ GeV	$p_T = 150$ GeV	$p_T = 2$ GeV	$p_T = 300$ GeV
$\delta_\mu^{\rm NLO}$	20.9%	27.2%	28.7%	34.0%
$\delta_\mu^{\rm NLO+NLL}$	17.2%	16.3%	16.9%	15.7%
	min. $\simeq$ 1.6%	(@ $p_T \sim 45$ GeV)	min. $\simeq$ 2.0%	(@ $p_T \sim 80$ GeV)

C. Invariant mass distribution

In this subsection, we discuss the threshold resummation effect on the invariant mass distribution of the scalar-pseudoscalar pair produced at the 13 TeV LHC in the type-I 2HDM. The central scale is set to the invariant mass of the final-state scalar-pseudoscalar pair, i.e., $\mu_0 = M$. In the upper panels of Figs. 5(a) and 6(a), we depict the invariant mass distributions of the $\phi^0 A^0$ system for both quark-initiated electroweak Drell-Yan production and gluon-initiated QCD production of $\phi^0 A^0$ at BP1 and BP2, respectively. The corresponding NLO and NLO+NLL QCD relative corrections to the Drell-Yan production channel are provided in the lower panels. The $\phi^0 A^0$ invariant mass distribution of the Drell-Yan channel increases rapidly near the production threshold, and then decreases consistently after reaching its maximum, with the increment of M. It peaks at $M \sim 450$ GeV for BP1 and $M \sim 1150$ GeV for BP2, respectively, at both LO

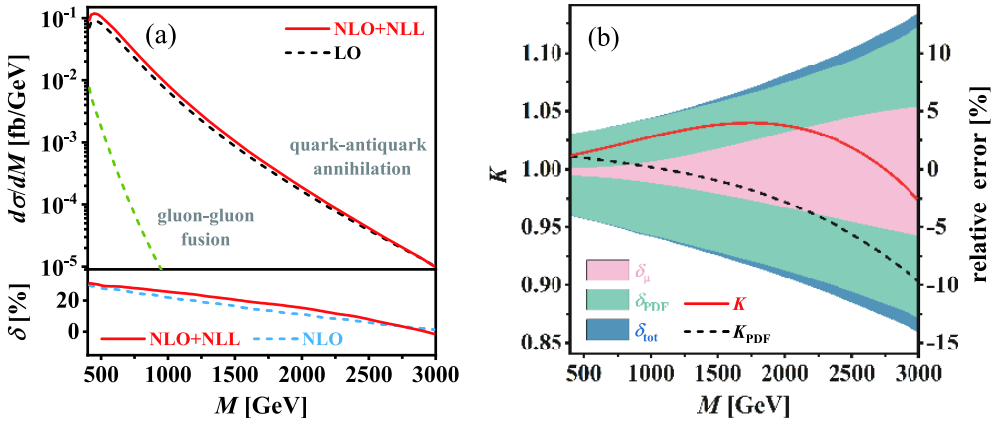

Fig. 5. (color online) (a) Invariant mass distribution of final-state ϕ^0A^0 and (b) factorization K-factors (K and $K_{\rm PDF}$) as well as theoretical relative errors (δ_μ, $\delta_{\rm PDF}$, and $\delta_{\rm tot}$) for ϕ^0A^0 associated production at $\sqrt{s}=13$ TeV LHC in type-I 2HDM at the benchmark point BP1.

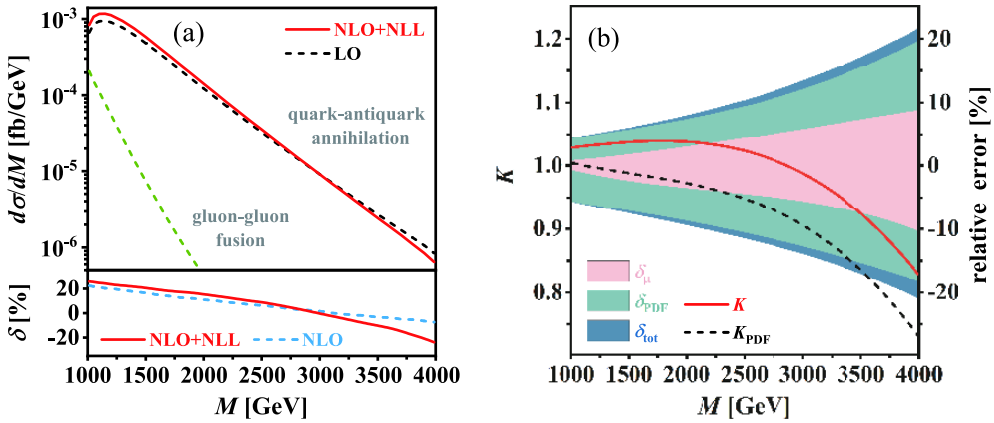

Fig. 6. (color online) Same as Fig. 5 but at BP2.

and NLO+NLL accuracies. Compared to the Drell-Yan channel, the ϕ^0A^0 invariant mass distribution of the gluon-gluon fusion channel is much smaller, and decreases more quickly with the increment of M. The ratio of the differential cross sections of the two channels, $d\sigma_{gg}/d\sigma^{\rm NLO+NLL}$, is approximately 8.1% at $M=400$ GeV for BP1 and 24.9% at $M=1000$ GeV for BP2, respectively, and approaches zero rapidly as the increase of M. It implies that the contribution from the gluon-gluon fusion channel is indispensable near the production threshold, but negligible in the high invariant mass region. The NLO and NLO+NLL QCD relative corrections ($\delta^{\rm NLO}$ and $\delta^{\rm NLO+NLL}$) to the Drell-Yan channel decrease gradually with the increment of M. They decrease from 29.8% to 1.4% and from 31.0% to −1.3%, respectively, as M increases from 400 GeV to 3 TeV at BP1, and vary correspondingly in the range of −7.3% ~ 22.4% and −23.9% ~ 25.9% as $M\in[1,4]$ TeV at BP2.

To further demonstrate the full NLL resummation effect and the impact of the threshold-resummation improved PDFs on the ϕ^0A^0 invariant mass distribution of the Drell-Yan channel, we plot the factorization K-factors K and $K_{\rm PDF}$ as functions of M in Figs. 5(b) and 6(b) for BP1 and BP2, respectively. The theoretical errors from scale variation and PDFs as well as their combination, i.e., δ_μ, $\delta_{\rm PDF}$, and $\delta_{\rm tot}$, are also displayed in these two figures. At the benchmark point BP1, K increases slowly from 1.01 to 1.04 as the increment of M from 400 GeV to 1.7 TeV, and then gradually decreases to 0.97 as M increases to 3 TeV. The full NLL resummation correction enhances the NLO QCD corrected invariant mass distribution of ϕ^0A^0 in the region of $M<2.7$ TeV, but it would reduce the invariant mass distribution at sufficiently high invariant mass. However, $K_{\rm PDF}$, which quantitatively reflects the impact of the threshold-resummation improved PDFs, decreases consistently from 1.01 to 0.90 as M varies from 400 GeV to 3 TeV. $K_{\rm PME}$, which describes the NLL resummation effect from the partonic matrix element and is calculated by $K/K_{\rm PDF}$, shows the opposite tendency compared to $K_{\rm PDF}$: it increases monotonically from 1.00 to 1.08 with the increment of M. At the benchmark point BP2, K is fairly stable in the range of 1 TeV $< M <$ 2 TeV; it reaches its maximum of around 1.04 at $M\sim1.8$ TeV and subsequently decreases to 0.83 as M increases to 4 TeV. Simultaneously, a global suppression induced by the threshold-resummation im-

proved PDFs can be clearly observed in the invariant mass distribution. Such suppression effect is very small and could be neglected at relatively low invariant mass, but becomes more and more apparent as the increasing of M. At $M = 4$ TeV, $K_{\rm PDF} = 0.73$; the contribution from the threshold-resummation improved PDFs is more notable at high invariant mass compared to the NLO QCD correction. On the contrary, $K_{\rm PME}$ increases from 1.02 to 1.13 as M increases from 1 to 4 TeV. In the high invariant mass region, the contribution from the threshold-resummation improved PDFs is the dominant correction compared to the NLO QCD correction and the NLL resummation correction from the partonic matrix element. For example, at $M = 4$ TeV, $K_{\rm PDF} - 1 = -27\%$, $\delta^{\rm NLO} = -7.3\%$ and $K_{\rm PME} - 1 = 13\%$, respectively.

V. SUMMARY

Searching for BSM Higgs bosons is an important task at the LHC and future high-energy colliders. In this study, we comprehensively analyze the scalar-pseudoscalar pair production at the 13 TeV LHC at the alignment limit in the type-I 2HDM. The Collins-Soper-Sterman resummation approach and the factorization method are employed to resum the NLL contributions and to evaluate the impact of the threshold-resummation improved PDFs, respectively, when addressing the quark-initiated Drell-Yan production channel. Both the integrated cross section and the differential distributions with respect to the transverse momentum and invariant mass of the produced scalar-pseudoscalar pair are provided. For quark-antiquark annihilation channel, the NLO QCD relative correction can exceed 30% in the low Higgs mass region, but decreases rapidly as the increment of m_{ϕ^0} and m_{A^0}. The relative correction induced by the threshold-resummation improved PDFs and the NLL resummation correction from the partonic matrix element, $K_{\rm PDF} - 1$ and $K_{\rm PME} - 1$, are insensitive to the mass splitting between ϕ^0 and A^0, and decreases and increases respectively with the increment of Higgs mass. They could be neglected compared to the NLO QCD correction in the low invariant mass region, but become increasingly important with the increment of the invariant mass of $\phi^0 A^0$, and can even predominate in the high invariant mass region. Moreover, the anomalous behavior of the NLO QCD corrected transverse momentum distribution in the small-p_T region can be resolved, and the scale uncertainty can be heavily reduced, especially in the intermediate-p_T region, by including the NLL resummation correction. Compared to the quark-initiated Drell-Yan channel, the contribution from the gluon-gluon fusion channel is negligible in the high invariant mass region, but indispensable and even comparable to the NLO QCD correction near the production threshold.

References

[1] G. Aad *et al*. (ATLAS Collaboration), Phys. Lett. B **716**, 1 (2012), arXiv:1207.7214[hep-ex]
[2] S. Chatrchyan *et al*. (CMS Collaboration), Phys. Lett. B **716**, 30 (2012), arXiv:1207.7235[hep-ex]
[3] G. C. Branco, P. M. Ferreira, L. Lavoura *et al*., Phys. Rept. **516**, 1 (2012), arXiv:1106.0034[hep-ph]
[4] B. Hespel, D. López-Val, and E. Vryonidou, *Higgs pair production via gluon fusion in the Two-Higgs-Doublet Model*, JHEP **09**, 124, arXiv: 1407.0281[hep-ph]
[5] R. Enberg, W. Klemm, S. Moretti *et al*., Phys. Lett. B **764**, 121 (2017), arXiv:1605.02498[hep-ph]
[6] A. M. Sirunyan *et al*. (CMS Collaboration), JHEP **03**, 055 (2020), arXiv:1911.03781 [hep-ex]
[7] G. Aad *et al*. (ATLAS Collaboration), Eur. Phys. J. C **81**, 396 (2021), arXiv:2011.05639[hep-ex]
[8] S. Dawson, S. Dittmaier, and M. Spira, Phys. Rev. D **58**, 115012 (1998), arXiv:hep-ph/9805244[hep-ph]
[9] J. C. Collins and D. E. Soper, Nucl. Phys. B **197**, 446 (1982)
[10] J. C. Collins and D. E. Soper, Nucl. Phys. B **193**, 381 (1981)
[11] J. C. Collins and D. E. Soper, Erratum: Nucl. Phys. B **213**, 545 (1983)
[12] J. C. Collins, D. E. Soper, and G. Sterman, Nucl. Phys. B **250**, 199 (1985)
[13] G. Sterman, Nucl. Phys. B **281**, 310 (1987)
[14] S. Catani and L. Trentadue, Nucl. Phys. B **327**, 323 (1989)
[15] S. Catani, M. L. Mangano, P. Nason *et al*., Nucl. Phys. B **478**, 273 (1996), arXiv:hep-ph/9604351[hep-ph]
[16] S. Catani, D. de Florian, and M. Grazzini, Nucl. Phys. B **596**, 299 (2001), arXiv:hepph/0008184[hep-ph]
[17] G. Bozzi, S. Catani, D. de Florian *et al*., Nucl. Phys. B **737**, 73 (2006), arXiv:hepph/0508068[hep-ph]
[18] W. Beenakker, C. Borschensky, M. Krämer *et al*., Eur. Phys. J. C **76**, 53 (2016), arXiv:1510.00375[hep-ph]
[19] D. Eriksson, J. Rathsman, and O. Stål, Comput. Phys. Commun. **181**, 833 (2010), arXiv:0902.0851[hep-ph]
[20] G. 't Hooft and M. Veltman, Nucl. Phys. B **44**, 189 (1972)
[21] S. Catani and M. H. Seymour, Nucl. Phys. B **485**, 291 (1997)
[22] S. Catani and M. H. Seymour, Erratum: Nucl. Phys. B **510**, 503 (1998), arXiv:hepph/9605323[hep-ph]
[23] B. W. Harris and J. F. Owens, Phys. Rev. D **65**, 094032 (2002), arXiv:hep-ph/0102128[hep-ph]
[24] S. Dulat, T.-J. Hou, J. Gao *et al*., Phys. Rev. D **93**, 033006 (2016), arXiv:1506.07443[hep-ph]
[25] H. Contopanagos, E. Laenen, and G. Sterman, Nucl. Phys. B **484**, 303 (1997), arXiv:hep-ph/9604313[hep-ph]
[26] S. Catani and L. Trentadue, Nucl. Phys. B **353**, 183 (1991)
[27] N. Kidonakis and G. Sterman, Nucl. Phys. B **505**, 321 (1997), arXiv:hep-ph/9705234[hep-ph]
[28] N. Kidonakis, G. Oderda, and G. Sterman, Nucl. Phys. B **525**, 299 (1998), arXiv:hep-ph/9801268[hep-ph]
[29] A. Vogt, Phys. Lett. B **497**, 228 (2001), arXiv:hep-ph/0010146[hep-ph]
[30] M. Krämer, E. Laenen, and M. Spira, Nucl. Phys. B **511**,

523 (1998), arXiv:hep-ph/9611272[hep-ph]
[31] S. Catani, D. de Florian, and M. Grazzini, *Higgs production in hadron collisions: soft and virtual QCD corrections at NNLO*, JHEP **05**, 025, arXiv: hep-ph/0102227[hep-ph]
[32] A. Kulesza, G. Sterman, and W. Vogelsang, Phys. Rev. D **66**, 014011 (2002), arXiv:hep-ph/0202251[hep-ph]
[33] G. Bozzi, B. Fuks, and M. Klasen, Nucl. Phys. B **777**, 157 (2007), arXiv:hep-ph/0701202[hep-ph]
[34] L. G. Almeida, G. Sterman, and W. Vogelsang, Phys. Rev. D **80**, 074016 (2009), arXiv:0907.1234[hep-ph]
[35] E. Laenen, G. Sterman, and W. Vogelsang, Phys. Rev. Lett. **84**, 4296 (2000), arXiv:hep-ph/0002078[hep-ph]
[36] W. Furmanski and R. Petronzio, Z. Phys. C **11**, 293 (1982)
[37] J. Debove, B. Fuks, and M. Klasen, Nucl. Phys. B **842**, 51 (2011), arXiv:1005.2909[hep-ph]
[38] B. Fuks, M. Klasen, D. R. Lamprea *et al*., Eur. Phys. J. C **73**, 2480 (2013), arXiv:1304.0790[hep-ph]
[39] M. Bonvini, S. Marzani, J. Rojo *et al*., *Parton distributions with threshold resummation*, JHEP **09**, 191, arXiv: 1507.01006[hep-ph]
[40] B. Fuks, M. Klasen, D. R. Lamprea *et al*., *Revisiting slepton pair production at the Large Hadron Collider*, JHEP **01**, 168, arXiv: 1310.2621[hep-ph].
[41] T. Hahn and M. Pérez-Victoria, Comput. Phys. Commun. **118**, 153 (1999), arXiv:hep-ph/9807565[hep-ph]
[42] T. Hahn, Comput. Phys. Commun. **140**, 418 (2001), arXiv:hep-ph/0012260[hep-ph]
[43] G. J. van Oldenborgh, Comput. Phys. Commun. **66**, 1 (1991)
[44] P. A. Zyla *et al*. (Particle Data Group), Prog. Theor. Exp. Phys. **2020**, 083C01 (2020)
[45] B. Grinstein, C. W. Murphy, and P. Uttayarat, *One-loop corrections to the perturbative unitarity bounds in the CP-conserving two-Higgs doublet model with a softly broken $\mathbb{Z}_2$ symmetry*, JHEP **06**, 070, arXiv: 1512.04567[hep-ph].
[46] S. Nie and M. Sher, Phys. Lett. B **449**, 89 (1999), arXiv:hep-ph/9811234[hep-ph]
[47] A. G. Akeroyd, A. Arhrib, and E. Naimi, Phys. Lett. B **490**, 119 (2000), arXiv:hep-ph/0006035[hep-ph]
[48] F. Mahmoudi, Comput. Phys. Commun. **180**, 1579 (2009), arXiv:0808.3144[hep-ph]
[49] P. Bechtle, S. Heinemeyer, O. Stål *et al*., Eur. Phys. J. C **74**, 2711 (2014), arXiv:1305.1933[hep-ph]
[50] P. Bechtle, D. Dercks, S. Heinemeyer *et al*., Eur. Phys. J. C **80**, 1211 (2020), arXiv:2006.06007[hep-ph]
[51] T.-J. Hou, K. Xie, J. Gao *et al*., *Progress in the CTEQ-TEA NNLO global QCD analysis*, (2019), arXiv: 1908.11394[hep-ph]
[52] J. Pumplin, D. Stump, R. Brock *et al*., Phys. Rev. D **65**, 014013 (2001), arXiv:hep-ph/0101032[hep-ph]